Received: 22 November 2016 | Accepted: 13 August 2017

DOI: 10.1111/1365-2435.12986

RESEARCH ARTICLE

Functional Ecology | BRITISH ECOLOGICAL SOCIETY

Axial xylem architecture of *Larix decidua* exposed to CO_2 enrichment and soil warming at the tree line

Angela Luisa Prendin[1] | Giai Petit[1] | Patrick Fonti[2] | Christian Rixen[3] | Melissa Autumn Dawes[2,3] | Georg von Arx[2,4]

[1]Dipartimento Territorio e Sistemi Agro-Forestali, Università degli Studi di Padova, Legnaro, PD, Italy

[2]Swiss Federal Institute for Forest, Snow and Landscape Research WSL, Birmensdorf, Switzerland

[3]WSL Institute for Snow and Avalanche Research SLF, Davos, Switzerland

[4]Climatic Change and Climate Impacts, Institute for Environmental Sciences, Geneva, Switzerland

Correspondence
Angela Luisa Prendin
Email: angelaluisa.prendin@studenti.unipd.it

Funding information
Swiss National Science Foundation from 2001–2005, Grant/Award Number: 31-061428.00; Swiss National Science Foundation from 2007–2010, Grant/Award Number: 315200-116861; Velux Foundation from 2007 to 2012, Grant/Award Number: 371; Swiss State Secretariat for Education, Research and Innovation SERI, Grant/Award Number: SBFI C14.0104 and C12.0100, WSL grant from 2012 to 2016

Handling Editor: Markku Larjavaara

Abstract

1. Trees continuously adjust their axial xylem structure to meet changing needs imposed by ontogenetic and environmental changes. These axial structure–function responses need to be coordinated among competing biophysical constraints to avoid failure of the xylem system. Here, we investigated if ontogeny or experimental manipulation of CO_2 and soil temperature influence these structure–function responses.
2. We performed detailed xylem cell anatomical quantification along the axis of 40-year-old *Larix decidua* trees planted at the Swiss tree line and exposed to a combination of elevated CO_2 (+200 ppm) and soil warming (+4°C) between 2001 and 2012. We assessed how mean hydraulic tracheid diameter (*D*h), the cell wall reinforcement ($(t/b)^2$), tracheid wall thickness (CWT) and the percent area of ray parenchyma (PERPAR)—proxies for hydraulic efficiency, hydraulic safety, biomechanical support and metabolic xylem functions, respectively—covary along the tree axis.
3. *D*h increased from the stem apex to base, strictly following a power function (R^2=0.81), independent from ontogeny and experimental treatments. In contrast, axial trends of $(t/b)^2$ and CWT were either influenced by treatment and/or ontogeny, or showed no axial trend (PERPAR). Additionally, we found that a larger *D*h only at the stem apex promoted primary and secondary growth.
4. Our approach of analysing xylem anatomical traits along the tree axis and across tree rings provides novel insights into xylem functional architecture and allows reconstructing xylem function over time. We conclude that the maintenance of hydraulic efficiency during ontogeny is very robust, that the tracheid diameter undergoes a strong apical control, and plays a fundamental role for assimilation and tree growth. Instead, the other functional traits more plastically vary with ontogeny and environmental changes.

KEYWORDS

axial scaling, cell wall thickness, elevated CO_2, ray parenchyma, soil warming, structure–function relationships, tracheid lumen size, tree-ring anatomy

1 | INTRODUCTION

Plants have developed different mechanisms to continuously adjust to environmental variability and changing needs and priorities. Short-term responses of physiological processes at different organizational levels are common to all plant types. However, especially for long-living trees that continuously increase in size and biomass, profound structural adjustments are necessary to meet changing requirements for transport, support and storage. In addition, many of these structural adjustments allow trees to acclimate to environmental variability and therefore to live for centuries or even millennia. Conversely, the legacy of past structural adjustments can constrain future responses of physiological processes (Anderegg et al., 2013; Meinzer, Lachenbruch, & Dawson, 2011). Thus, investigating how tree structures and their associated functions change over time and in relation to environmental variability provides a deeper understanding of tree growth and its determinants, which will ultimately help improve predictions of how forest ecosystems might be affected under different scenarios of climate change.

One emerging approach to gain such detailed structure–function insights is dendro-anatomy. Dendro-anatomy focuses on the quantitative assessment of the xylem tissues and cells, and the metrics or traits that can be derived and linked to specific xylem functions. The approach is based on the fact that xylem structural adjustments are permanently recorded and chronologically archived in the tree rings (Fonti et al., 2010), thus providing an explicit time frame in the retrospective analysis of the structure–function responses of trees to climate variability (Fonti & Jansen, 2012). In conifers, the xylem is mainly composed of tracheids and parenchyma cells, both of which have multiple functional roles. Tracheids are axially elongated cells that transport water from the roots to the canopy, provide mechanical support (Bouche et al., 2014; Choat, 2013; Hacke, 2015) and facilitate bending stiffness in the tree stem (Rosner & Karlsson, 2011). In contrast, parenchyma cells are living cells that are predominantly organized as rays in conifers, running radially from the bark towards the pith, thus physiologically integrating the xylem internally (Fonti, Tabakova, Kirdyanov, Bryukhanova, & von Arx, 2015) and with the phloem (Pfautsch, Hölttä, & Mencuccini, 2015; Spicer, 2014). Collectively, parenchyma cells play a major role for storage and transport of water, nutrients (Beeckman, 2016) and non-structural carbohydrates (NSC) (von Arx et al., 2017). In addition, parenchyma cells contribute to the regulation of the xylem hydraulics, e.g. through the osmo-regulation of axial and radial gradients of water potential (Brodersen & McElrone, 2013; Lintunen et al., 2016) or by refilling embolized conductive elements (Nardini, Lo Gullo, & Salleo, 2011; Salleo, Trifilò, Esposito, Nardini, & Lo Gullo, 2009; Ziemińska, Westoby, & Wright, 2015).

Quantifying how the dimensions and abundance of tracheids and parenchyma cells change within trees and in response to both increasing tree size and environmental variability might provide important insights into the plasticity of xylem functioning. Earlywood tracheids are thin-walled and characterized by wide lumina that contribute most to the efficiency of water transport (Domec & Gartner, 2002). Hydraulic efficiency is commonly estimated by the xylem-specific conductivity (Mencuccini, Grace, & Fioravanti, 1997) and by the hydraulic lumen diameter (Rosner & Karlsson, 2011). While both of these metrics can be estimated from tracheid lumen properties, this approach ignores the fact that more than 60% of flow resistance resides in the tracheid walls as the water moves from one tracheid to the next through the bordered pit pores (Hacke, 2015). However, the proportion of lumen vs. pit resistance seems to be more or less constant and independent from tracheid size (Pittermann, Sperry, Wheeler, Hacke, & Sikkema, 2006). In contrast, the latewood tracheids with narrow lumina and thicker cell walls rather store water (Domec & Gartner, 2002; Mcculloh, Johnson, Meinzer, & Woodruff, 2014) and, most importantly, provide biomechanical support (Finto, Schimleck, & Daniels, 2012; Koubaa, Zhang, & Makni, 2002). Indeed, the latewood cell wall thickness (CWT) is a key determinant for latewood density in conifers (Björklund et al., 2017). The latewood density strongly contributes to the overall wood density (Jyske, Mäkinen, & Saranpää, 2008), which is considered a good proxy for mechanical support and stiffness (Domec, Warren, Meinzer, & Lachenbruch, 2009; Rosner & Karlsson, 2011). Moreover, the tracheid's thickness-to-span ratio, also referred to as cell wall reinforcement ($(t/b)^2$), is considered a primary determinant of the resistance to hydraulic failure by implosion (Hacke, Sperry, Pockman, Davis, & McCulloh, 2001; Pittermann et al., 2006). Hydraulic failure by implosion can occur when a water-filled conduit physically collapses owing to the pressure differences between its lumen and an adjacent air-filled conduit (Hacke et al., 2001). Both $(t/b)^2$ and percentage of latewood were shown to well correlate with embolism resistance in different organs (Domec et al., 2009) and across species (Bouche et al., 2014). The percentage of ray parenchyma can be used as a proxy for the amount of metabolically active tissue, with more parenchyma indicating greater vigour within a species (von Arx, Arzac, Olano, & Fonti, 2015). Studying how characteristics of tracheids and abundance of parenchyma cells change within trees and in response to both increasing tree size and environmental variability might thus provide important insights into the plasticity of xylem functioning.

Our understanding of the variability of functionally relevant cell anatomical traits along the tree stem and root during ontogeny is still fragmentary. Theoretical models predict that different anatomical traits should vary according to strict allometric axial scaling defined by biophysical constraints that are related to tree size (Savage et al., 2010; West, Brown, & Enquist, 1999). Besides biophysical constraints, such as limiting the risk of hydraulic failure while maintaining an adequate capacity for water transport despite the increasing xylem tension with greater tree height (Domec et al., 2008), minimizing the carbon cost per unit leaf area may also be important (Olson et al., 2014). However, detailed empirical studies of within-plant patterns have mostly been limited to the axial variability of tracheid lumen diameter (but see Lazzarin et al., 2016). Both models and observations show that tracheid lumen diameter increases from the stem apex to the base following a power-like trajectory ($y = a \cdot x^b$), with a scaling exponent generally converging towards a value of c. 0.2 irrespective of species, environment or ontogenetic stage (Anfodillo, Petit, & Crivellaro, 2013; Olson et al., 2014). This pattern is linked to the physical law of Hagen and Poiseuille, according to which hydraulic conductance increases with conduit

lumen diameter to the fourth power (Tyree & Zimmermann, 2002). Relatively small changes in tracheid lumen diameter therefore scale up to a large difference in xylem-specific conductivity. Consequently, the progressively wider conduits towards the base confine most of the resistance and thus most of the tension within short distance from the apex (Petit & Anfodillo, 2009). This hydraulic architecture makes the pathway length hydraulic resistance mostly independent from tree height (Petit & Anfodillo, 2009; West et al., 1999). In contrast, there is still little knowledge about the axial variability of other important xylem structure–function relationships. A few empirical studies have reported an increase in cell wall thickness (e.g. Myburg, Lev-Yadun, & Sederoff, 2013) with increasing cambial age (Larson, 1963; Lundgren, 2004; Mitchell & Denne, 1997; Wimmer, 2002), likely following the pattern of *D*h. While the cell wall reinforcement ($(t/b)^2$) decreased with tree age but increased with height (Domec et al., 2009). A constant ray area and a decline of ray volume with cambial age was found in previous studies (Baker, Spicer, & Gartner, 2000; Bannan, 1937) but only little information is available on the sensitivity of ray parenchyma tissue to environmental conditions (Olano, Arzac, García-Cervigón, von Arx, & Rozas, 2013; von Arx et al., 2017). Further, there is still a lack of knowledge about how these and other functional traits covary both within the tree (e.g. Bouche et al., 2014; Lachenbruch & McCulloh, 2014; Pittermann et al., 2006) and over time, and thus we have only a limited understanding of how competing biophysical constraints, functional priorities and trade-offs are modulated by ontogenetic development and environmental conditions (Bittencourt, Pereira, & Oliveira, 2016; Gleason et al., 2016).

In this study, we retrospectively analysed the plasticity of functionally relevant xylem anatomical traits along the tree axis. As a study framework, we selected an experimental site at an upper alpine tree line. This temperature-limited ecotone is expected to be one of the terrestrial areas that is most sensitive to climate change, and it has therefore become a focus of recent research (Dawes et al., 2015; Harsch, Hulme, McGlone, & Duncan, 2009; Körner, 2012). This is the reason why tree lines are particularly suitable for investigating the mechanisms of xylem growth responses to environmental changes (e.g. Fatichi, Leuzinger, & Körner, 2014; Fatichi, Rimkus, Burlando, Bordoy, & Molnar, 2013; Petit, Anfodillo, Carraro, & Grani, 2011). The tree line trees selected for this study represent a subset of the 20 *L. decidua* exposed to a long-term experimental manipulation combining free air CO_2 enrichment (FACE) and soil warming (Dawes et al., 2015; Hättenschwiler et al., 2002). Previous analyses of *L. decidua* responses showed a stimulation of primary and secondary growth in stems and roots by the CO_2 enrichment (Dawes et al., 2011, 2015; Handa, Körner, & Hättenschwiler, 2006), which was partially explained by a larger leaf canopy resulting in increased photosynthetic carbon assimilation (Streit, Siegwolf, Hagedorn, Schaub, & Buchmann, 2014), while the experimental soil warming did not stimulate above- or belowground growth of *L. decidua* (Dawes et al., 2015). Building upon this knowledge from previous studies at this site, we used a representative subset of the experimental *L. decidua* trees to compare how the axial trends of four xylem functional traits related to hydraulic efficiency and safety, biomechanical support, and metabolic requirements vary within annual rings from the stem apex to the roots. In doing so, we specifically aimed to identify priorities and trade-offs among different xylem functions and to determine if ontogeny or treatments influence these relationships. We hypothesized that (1) hydraulic traits are prioritized over mechanical traits, as the former seem to limit tree height (Koch, Sillett, Jennings, & Davis, 2004; Niklas, 2007; Niklas & Spatz, 2004); (2) there are trade-offs between hydraulic efficiency and safety as approximated by cell wall reinforcement ($(t/b)^2$) at the within-ring level because wide and thick-walled earlywood tracheids would require high carbon costs; and (3) there are differences in trend plasticity, with the prioritized traits showing less plasticity during ontogeny and in response to treatments.

2 | MATERIALS AND METHODS

2.1 | Study site, experimental setup and tree selection

The study included *L. decidua* Miller trees from a long-term manipulation experiment located at 2180 m a.s.l., just above the current tree line (Barbeito, Dawes, Rixen, Senn, & Bebi, 2012), within the 40-year old Stillberg afforestation site near Davos, Switzerland (9°52′E, 46°46′N). The trees were on average 1.5 m tall in 2001 and 2.6 m in 2012 (Dawes et al., 2011) and spaced by >80 cm between stems of neighbouring trees, surrounded by dense understory vegetation dominated by ericaceous dwarf shrubs (Dawes et al., 2015; Hättenschwiler et al., 2002). The soil is classified as a Ranker (U.S. system: Lithic Haplumbrept) with a 10-cm-deep organic top soil over siliceous (Paragneis) bedrock (Schönenberger & Frey, 1988). Long-term average annual precipitation is 1,050 mm, mean maximum snow depth is 1.50 m, mean annual temperature is 1.4°C, and average January and July temperatures are −5.8°C and 9.4°C, respectively (Dawes et al., 2015). Climate conditions varied during the 4-year pre-treatment period and the 9 years of experimental CO_2 enrichment (Dawes et al., 2011), but no correlation was found between ring growth and the measured climate variables (Dawes et al., 2011; Handa et al., 2006). The growing season starts approximately on 15 June with bud break of *L. decidua* and ends on 25 September with needle senescence of *L. decidua*, thus lasting for c. 110 days (Hättenschwiler et al., 2002). The manipulation experiment was performed between 2001 and 2012 and included different combinations of FACE and soil warming (Table 1). CO_2 enrichment (+200 ppm higher than ambient CO_2 concentration) was performed from 2001 to 2009 and soil warming (+4°C at 5 cm depth) was applied using heating cables on the soil surface (see Dawes et al., 2015; Hagedorn et al., 2010; Hättenschwiler et al., 2002 for details about the experimental setup).

For this study, we used eight *L. decidua* trees, with two individuals per treatment combination: A_{2001}, A, EC, SW, ECSW, PECSW and PEC (Table 1). The study trees were selected to be representative for the tree responses to each treatment based on previous results (see above), while considering the presence of a leader shoot, lack of mechanical and/or herbivore damage, lack of snow mould and similar tree height at the beginning of the experiment.

TABLE 1 Timeline of the treatments and their combinations during the free air CO_2 enrichment (FACE) and soil warming experiment at Stillberg (Davos, Switzerland)

	Trees	1983–2000	2001	2002	2003	2004	2005	2006	2007	2008	2009	2010	2011	2012
Combined treatments	E1L1	A_{2001}	EC						ECSW			PECSW		
	E2L2													
	E1L2	A_{2001}	EC									PEC		
	E3L1													
	A1L1	A_{2001}	A						SW					
	A2L2													
	A1L2	A_{2001}	A											
	A2L1													

A_{2001}, ambient conditions before the beginning of the experiment; A, ambient conditions (control); EC, elevated CO_2; SW, soil warming, ECSW, elevated CO_2 and soil warming, PECSW, post elevated CO_2 and soil warming; PEC, post elevated CO_2 at ambient conditions.

2.2 | Reconstruction of axial and radial growth

To capture the temporal variability of xylem anatomical traits along the stem axis, we reconstructed the apex-to-root axial trend within each tree ring to provide an annual resolution (Figure S1). Thus, for each selected tree, we extracted a total of 20 discs along the stem (14) and the main root (6) (at 0–20 cm soil depth) for the reconstruction of both the axial and radial growth (Figure S1). The average distance between neighbouring discs was 11 cm. Tree-ring widths were measured along eight equally spaced radii per disc and cross-dated to assign each ring to its year of formation. Annual stem and root elongation (ΔH) was obtained by linearly interpolating the inter-disc distance divided by the age difference between neighbouring discs:

$$\Delta H = \frac{H_i - H_{i-1}}{RN_{i-1} - RN_i} \quad (1)$$

where H_i and RN_i are the height from the ground and the ring number of the *i*th disc, respectively (Figure S1). The average age difference between neighbouring discs varied from 1 to 14 years (with a median of 3 years) depending on the sample, thus giving reasonable confidence in the estimated annual stem elongation data (Figure S1). Finally, to reconstruct the axial position at the time of ring formation, for each annual ring within a given disc we calculated the distance from the stem apex (L) as the difference between the reconstructed tree height and the distance from the ground (for root discs L was calculated as the sum of tree height and axial distance from the ground).

2.3 | Anatomical measurements

Xylem cell anatomical measurements were performed using image analysis for a subset of the stem discs. In total, we selected ten axially well-distributed discs per tree, six from the stem and four from the roots (Figure S2). We followed the standard protocol for cutting micro-sections and collecting high-resolution images proposed by von Arx, Crivellaro, Prendin, Čufar, and Carrer (2016). From each disc, we extracted radial wood samples from opposite radii (Figure S2) and produced 10–15 μm thick cross-sections using a rotary microtome (Leica RM2245, Leica Biosystems, Nussloch, Germany). In addition, for ray parenchyma quantification (see below), we cut three tangential sections from each wood sample within the annual rings formed in 2000, 2006 and 2011 to include years from all the different treatment combinations (Table 1). All sections were stained with safranin and astrablue and permanently fixed with Eukitt (BiOptica, Milan, Italy). Overlapping images of the cross-sections and tangential sections were captured at 100× magnification using a light microscope connected to a digital camera (Nikon Eclipse 80i, Nikon, Tokyo, Japan), and then stitched using PTGui (version 8.3.3, New House Internet Services B.V., Rotterdam, NL) to obtain high-resolution images (2.07 pixels/μm). Image analysis was performed with ROXAS version 2.1 (von Arx & Carrer, 2014; von Arx & Dietz, 2005) which provided ring width and several measurements of cell anatomical features such as tracheid

lumen area and wall thickness from cross-sections (Prendin, Petit, & Carrer et al., 2017) and ray cell lumen area from tangential sections (see Figure S3). In total, we produced annual anatomical trait values (see below) for *c*. 1300 rings, based on measurements from >5 million tracheids. Compression wood rings were excluded from analysis.

2.4 | Functional anatomical traits

For each annual ring of each disc, we derived xylem functional traits using the aforementioned basic anatomical measurements (Table 2). For the functional traits calculated on earlywood (EW) and latewood (LW) tissue, tracheids were assigned to each tissue based on Mork's index, i.e. the ratio between twice the double-cell wall thickness and the lumen diameter (Denne, 1988). As a proxy for the hydraulic efficiency, we used the mean hydraulic diameter (*D*h), i.e. the lumen diameter corresponding to the mean hydraulic conductivity among all tracheids (Kolb & Sperry, 1999; Sperry, Nichols, Sullivan, & Eastlack, 1994). *D*h was calculated separately for the above-ground (Dh_{STEM}) and below-ground (Dh_{ROOT}) organs to account for their different demands and constraints. In addition, we calculated *D*h of the apex (Dh_{APEX}) due to its importance as the starting point for the axial tracheid widening. As an indicator of the hydraulic safety from cell implosion, we used the 5th percentile of cell wall reinforcement ($(t/b)^2$) (Hacke et al., 2001) (corresponding to the widest and most implosion-prone tracheids), where *t* is the double-cell wall thickness and *b* is the lumen diameter of the tracheid measured perpendicularly to the double-cell wall thickness. This produced two values per tracheid, one with radial and one with tangential orientation of lumen diameter. For each tracheid, the smaller of the two values was used to better reflect the risk of cell implosion. The mechanical support function of the xylem was estimated by the mean cell wall thickness of latewood tracheids (CWT_{LW}), as well as by the percentage of latewood. As a proxy for the metabolically active tissue, we considered the percent area of ray parenchyma (PERPAR; von Arx et al., 2015), measured here as the sum of ray cell lumen areas divided by the tangential section area (*c*. 5 mm^2, see Figure S3). To account for the different demands and constraints, above- and below-ground organs we calculated separately as $PERPAR_{STEM}$ and $PERPAR_{ROOT}$.

Additionally, we devised the 'hydraulic carbon use efficiency' index (HCUE) to express the hydraulic return for a given carbon investment. HCUE was calculated for each ring as the ratio of the accumulated theoretical conductance of all tracheids (*Kh* according to Poiseuille's law, Tyree & Ewers, 1991) to the accumulated wall area of all tracheids

TABLE 2 Acronyms and descriptions of variables used in this study

Variable	Description	Function	Reference
Descriptive			
L (cm)	Distance from the apex	–	
H (cm)	Tree height	–	
Functional traits			
*D*h (μm)	Tracheid hydraulic diameter	Hydraulic efficiency	Kolb & Sperry (1999)
Dh_{STEM} (μm)	In the stem		
Dh_{ROOT} (μm)	In the root		
Dh_{APEX} (μm)	In a ring corresponding to cambial age = 1		
$(t/b)^2$	Cell wall reinforcement (in this study: 5th percentile of values calculated for the earlywood tracheids)	Hydraulic safety	Hacke et al. (2001)
CWT_{LW} (μm)	Cell wall thickness of latewood tracheids (proxy for density)	Mechanical support	Myburg et al. (2013)
CWA (μm^2)	Cell wall area accumulated for the entire ring	Mechanical support	
PERPAR (%)	Percentage area of ray parenchyma cells on tangential section:	Metabolic functions, e.g. capacity of carbon & water storage and radial transport	Spicer (2014); von Arx et al. (2015)
$PERPAR_{STEM}$ (%)	In the stem		
$PERPAR_{ROOT}$ (%)	In the root		
Kh ($kg\ m^{-1}\ MPa^{-1}\ s^{-1}$)	Total conductivity	Hydraulic efficiency	Tyree & Zimmermann (2002)
Economics			
Hcue ($kg\ m^{-1}\ MPa^{-1}\ s^{-1}\ \mu m^{-2}$)	Hydraulic carbon use efficiency: *Kh*/CWA	–	
Growth			
Δ*H* (cm)	Annual stem elongation	–	
RA (μm^2)	Ring area		
RAI	Annual ring area index (RA standardized to remove the general axial pattern)	–	

within the ring (CWA_{RING}). Finally, as a proxy for growth, the ring area (RA) of each ring (*c*. 1300) was estimated based on the ROXAS ring width measurements assuming a circular stem cross-section.

2.5 | Estimation of axial scaling and treatment effects

For each functional tracheid trait (*D*h, $(t/b)^2$, CWT_{LW}), we fitted linear, power and exponential functions to identify which function best described the axial scaling. Fitting was performed only for stem annual rings from trees that were not subject to any treatment (treatments A_{2001} and A, see Table 1) to avoid potential confounding treatment effects. In addition, to check for ontogenetic trends, we computed the scaling exponents ('slope') throughout the life of each tree using a model type II regression analysis with the reduced major axis (RMA) protocol in the lmodel2 R package (Legendre, 2014). We based this analysis on data from a moving window of three neighbouring tree rings to increase the number of axial points, which then did not allow us to additionally check for interactions between ontogeny and treatments. This analysis could only be performed with data from 2001 to 2012, thus not covering the first *c*. 30 years of tree growth. Similarly, we established the relationships among the functional traits (*D*h, $(t/b)^2$, CWT_{LW} and PERPAR) in terms of axial scaling and trait covariance by identifying the function (linear, power or exponential) that provided the highest R^2. The initial exploration of the covariance of the functional traits with the overall dataset revealed that the power functions fit best (data not shown). The covariance of functional traits in tree rings of different cambial age was then assessed with the best fitting function and evaluated for trends in the pairwise relationships during ontogeny and treatments. In addition, we tested the relationship between each functional trait (*D*h, $(t/b)^2$, CWT_{LW} and PERPAR) and each growth parameter ΔH and RAI (see Table 2).

Treatment effects on the axial patterns were tested using linear mixed-effects models fitted with restricted maximum likelihood (REML). We established a model for each response variable (Dh_{ROOT}, $(t/b)^2$, CWT_{LW}, PERPAR and HCUE), where distance from the apex (*L*), treatment combinations (see Table 1) and their interactions were included as fixed effects, and tree identity and disc height along the tree axis as random factors in all initial models, reflecting the experimental design and the sample collection. Response variables were $\log_{10}$-transformed to comply with assumptions of normality and homoscedasticity (Zar, 1999). For the Dh_{STEM} model, we additionally included Dh_{APEX} as a fixed effect to account for its known strong influence on Dh_{STEM} (Petit et al., 2011). For this model, we only considered annual rings for which apical data (defined as ≤1 cm from tree top) were available. The best model was chosen based on AICc using the maximum likelihood method (Zuur, Ieno, Walker, Saveliev, & Smith, 2009). When several models showed similar AICc values (ΔAICc < 2, Burnham & Anderson, 2002), they were refitted with the REML method to obtain estimates and significance values of effects, and the simplest model with significant fixed effects was chosen as the 'optimal' model. The significance of the fixed effects was tested with *F* tests (Pinheiro & Bates, 2000). When the target functional trait did not exhibit a significant axial trend, the difference between treatment combinations was tested with Tukey's Honest Significance test based on ANOVA. All analyses were performed using R (version 3.1.1; R Development Core Team, 2014), and linear mixed-effects models were run using the lme4 (Bates, Mächler, Bolker, & Walker, 2015) and MuMIn packages (Barton & Barton, 2013).

3 | RESULTS

3.1 | Axial scaling of xylem trait

The analysis of the functional trait variability along the whole tree axis using different parametric functions (Figure 1a–d) revealed that the power function provided the best fit to the data, with R^2 values ranging from 0.81 (*D*h) to 0.16 (CWT_{LW}) (Table 3). However, for CWT_{LW} the power function performed only slightly better than the linear and exponential ones. Tracheid hydraulic diameter (*D*h) increased continuously down the stem and further along the roots (see also the axial profile for the tree ring of 2011 for tree E3L1 shown in Figure 1a). This widening pattern was narrowly confined for the stem, thus indicating only small differences among individuals and no significant changes throughout ontogeny ($p = .81$, Figure 2a). For each year of growth, *D*h in the roots was larger than in the stem, generally increased with *L* at faster rates than in the stem, and showed more variation in the data ($R^2 = 0.10$) (Figure 1a).

The 5th percentile of cell wall reinforcement $(t/b)^2$ decreased continuously from the stem apex to the stem base and further below ground along the roots. In the stem, *L* explained 46% of the total variance in $(t/b)^2$ (Table 3), while in the roots this relationship was not significant ($p = .31$) (Figure 1b). Additionally, the scaling exponent (*b*) of the relationship of $(t/b)^2$ vs. distance from the apex (*L*) progressively decreased with tree age ($R^2 = 0.48$, $p < .001$, Figure 2b). The cell wall thickness of the latewood tracheids (CWT_{LW}) increased continuously from the stem apex to the base and further along the roots (Figure 1c). The inter-annual variability was substantial in this trait, as shown by the low R^2 of 0.16 for the stem (Table 3) and the non-significant

FIGURE 1 Axial variability of functional traits as a function of distance from the apex (*L*) along the stem and root of the eight investigated *Larix decidua* trees. Left panels show the axial trends of (a) hydraulic diameter (*D*h), (b) 5th percentile of cell wall reinforcement ($(t/b)^2$), (c) cell wall thickness of the latewood tracheids (CWT_{LW}) and (d) percentage of ray parenchyma (PERPAR). Each data point represents the trait value of a tree ring calculated for different positions along the tree axis (see Figures S1b and S2a), with filled and open grey circles for the stem and root data, respectively. As an arbitrary example, red points/dots represent the axial variability (stem and root combined) in the tree ring of 2011 for a single tree (E3L1). Solid lines show the best fitting curves, whose details are reported in Table 3. In the right panels (e–g), the black lines denote the linear regression lines of the $\log_{10}$-$\log_{10}$ transformed variables for each selected functional trait ((e): *D*h; (f): $(t/b)^2$, (g): CWT_{LW}) of control trees (A_{2001}, A). Coloured lines indicate the significant treatment effects (see Table 4 for details). (h) $M \pm 1$ *SE* of PERPAR grouped per treatment for stem (filled circles) and root (open squares), $^*p < .05$. See Tables 1 and 2 for explanations of acronyms

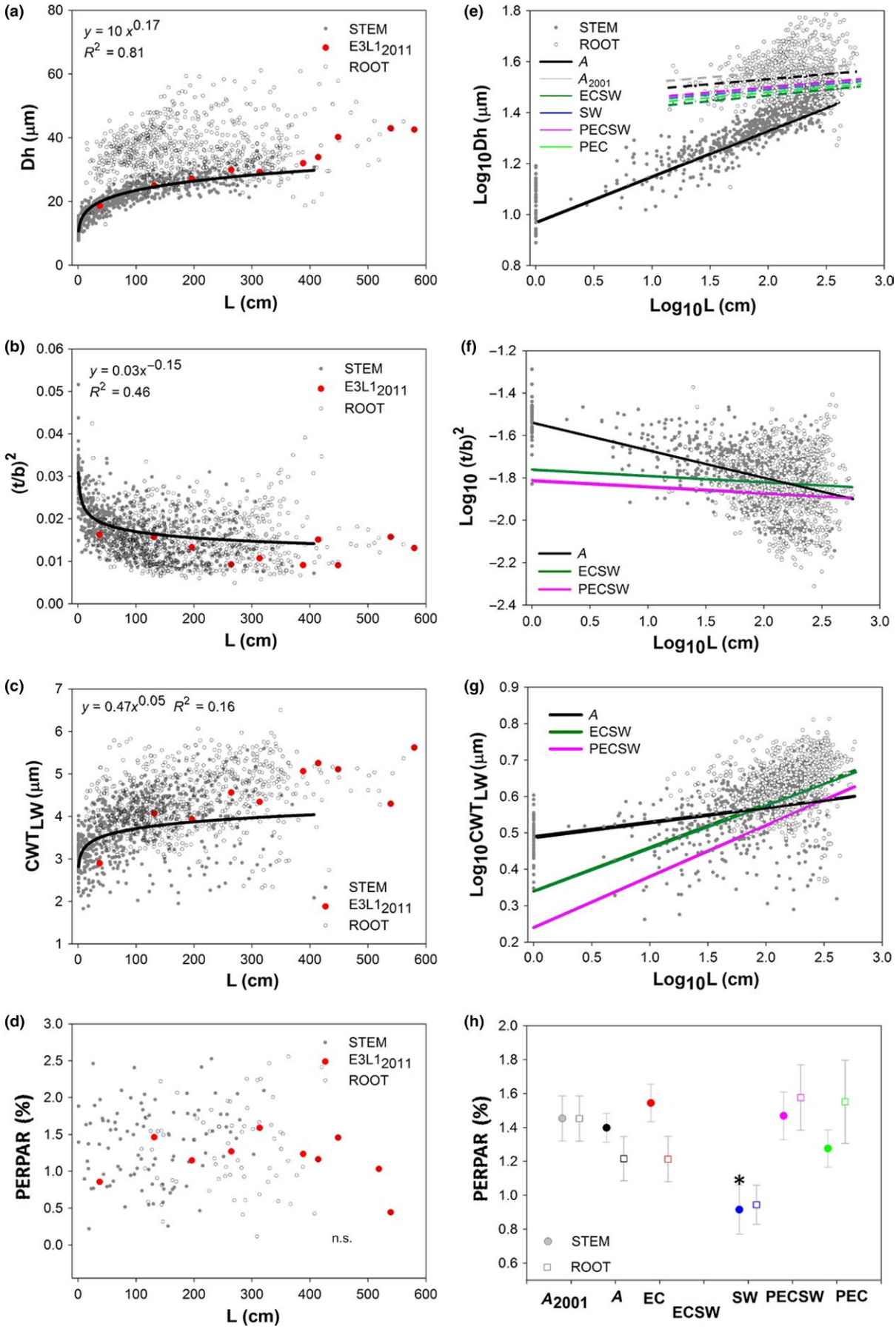
(a)
y = 10 x^0.17
R² = 0.81
STEM
E3L1 2011
ROOT
Dh (µm)
L (cm)
(b)
y = 0.03x^−0.15
R² = 0.46
STEM
E3L1 2011
ROOT
(t/b)²
L (cm)
(c)
y = 0.47x^0.05 R² = 0.16
CWT LW (µm)
STEM
E3L1 2011
ROOT
L (cm)
(d)
PERPAR (%)
STEM
E3L1 2011
ROOT
n.s.
L (cm)
(e)
STEM
ROOT
A
A 2001
ECSW
SW
PECSW
PEC
Log10 Dh (µm)
Log10 L (cm)
(f)
Log10 (t/b)²
A
ECSW
PECSW
Log10 L (cm)
(g)
A
ECSW
PECSW
Log10 CWT LW (µm)
Log10 L (cm)
(h)
PERPAR (%)
*
STEM
ROOT
A2001
A
EC
ECSW
SW
PECSW
PEC

relationship for the roots (p = .90). Furthermore, the scaling exponent b of the power function relating CWT_{LW} to L progressively increased with tree age (R^2 = 0.86, p < .001, Figure 2c). However, this ontogenetic trend was only significant when a power function was used but not when linear or exponential fitting was applied (p = .71 and p = .11, respectively). The percentage of latewood did not show an axial trend (Figure S4a) and was significantly related to CWT_{LW} (R^2 = 0.38 and R^2 = 0.09, p < .001, for stem and root, respectively; Figure S4b). The experimental design did not allow us to additionally test for treatment effects on the ontogenetic trend. The percent area of ray parenchyma (PERPAR) did not change significantly with distance from the apex in the stem (p = .53) and root (p = .83) (Figure 1d).

3.2 | Treatment effects on axial trait scaling

The linear mixed-effect models used to test for the importance of treatments on the axial scaling of Dh_{STEM} did not reveal any significant

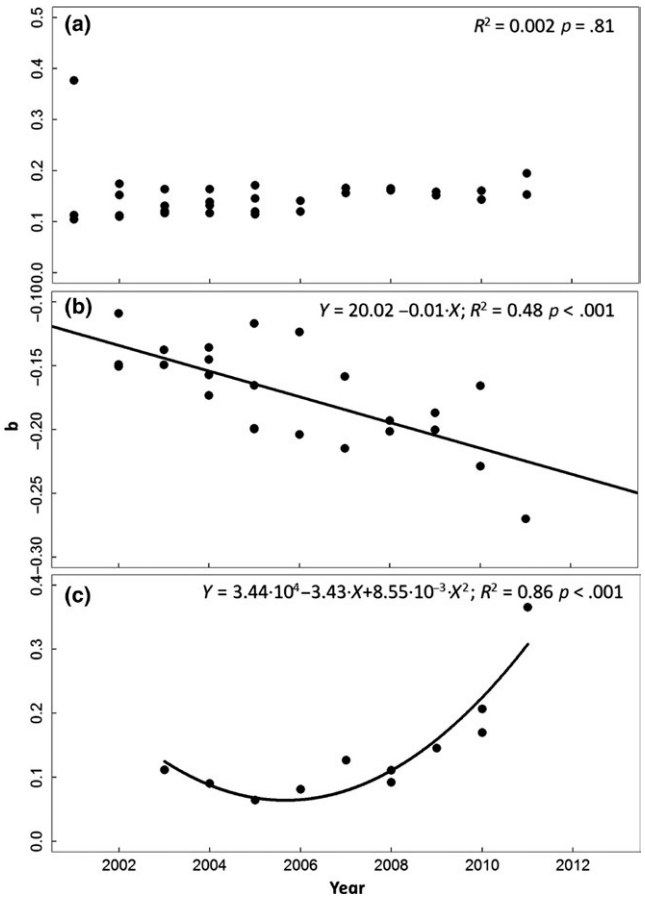

FIGURE 2 Ontogenetic variation of the power scaling exponent b, corresponding to the axial trend in the general equation $y = aL^b$, for (a) Dh, (b) $(t/b)^2$ and (c) CWT_{LW} of the two control trees throughout the experiment (A1L1, A1L2; see Table 1). Only stem data for the period from 2001 to 2012, corresponding to tree age of 28 to 39 years and tree height of *c*. 1.1 to 2.6–3.6 m (see Figure S1c), could be considered to avoid too few axial points for robust trend calculations. Solid curves indicate the best fitting regressions of the ontogenetic trend

TABLE 3 Linear, power and exponential fitting parameters (M ± 1 SE) a: y-intercept, b: slope), coefficient of determination (R^2) and significance (p) of the relationships assessed for the different trait variables. Relationships were only assessed for control trees not undergoing any CO_2 enrichment or soil warming treatment (A_{2001} and A; n = 8 trees until 2001, n = 4 from 2001 to 2006, n = 2 from 2007 to 2012). See Table 2 for explanations of acronyms

	Linear ($y = a + b \times x$)				Power ($\text{Log}_{10}(y) = \text{Log}_{10}(a) + b \times \text{Log}_{10}(x)$)				Exponential ($y = a + x^b$)			
	a	b	R^2	P	$\text{Log}_{10}(a)$	b	R^2	p	a	b	R^2	p
Axial variation												
Dh vs. L	14.90 ± 0.21	0.07 ± 2.25 × 10^{-3}	0.72	<.001	1.00 ± 0.01	0.17 ± 0.01	0.81	<.001	2.86 ± 0.02	2.18 × 10^{-3} ± 1.28 × 10^{-4}	0.66	<.001
$(t/b)^2$ vs. L	0.02 ± 4.17 × 10^{-4}	−5.63 × 10^{-5} ± 4.5 × 10^{-6}	0.31	<.001	−1.50 ± 0.02	−0.15 ± 0.01	0.46	<.001	−3.81 ± 0.04	−2.62 × 10^{-3} ± 3.35 × 10^{-4}	0.28	<.001
CWT_{LW} vs. L	3.35 ± 0.05	4.09 × 10^{-3} ± 5.35 × 10^{-4}	0.15	<.001	0.47 ± 0.01	0.05 ± 0.01	0.16	<.001	1.22 ± 0.03	1.02 × 10^{-3} ± 1.38 × 10^{-4}	0.15	<.001
Economics												
HCUE vs. L	1.64 × 10^{-15} ± 2.24 × 10^{-16}	2.52 × 10^{-17} ± 2.42 × 10^{-18}	0.25	<.001	−15.22 ± 0.04	0.46 ± 0.02	0.44	<.001	−2.99 ± 0.06	−0.03 ± 1.78 × 10^{-3}	0.21	<.001
Growth												
ΔH vs. Dh_{APEX}	−9.37 ± 7.88	1.78 ± 0.70	0.20	.017	−1.20 ± 0.61	2.02 ± 0.58	0.31	<.001	0.57 ± 0.91	0.16 ± 0.07	0.21	.007
RAI vs. Dh_{APEX}	0.71 ± 0.07	0.02 ± 0.01	0.34	<.001	−0.30 ± 0.07	0.27 ± 0.07	0.36	<.001	−0.29 ± 0.07	0.02 ± 6.20 × 10^{-3}	0.33	<.001

TABLE 4 Results of the optimal linear mixed-effect models predicting the treatment effects on the different functional and carbon cost traits and the interaction between treatment and $Log_{10}L$ (see methods for details). Numbers indicate the estimates ±1 *SE*. Significant terms are highlighted in bold. See Tables 1 and 2 for explanations of acronyms

	Functional traits				Carbon costs
Fixed effects	**Log_{10} Dh_{STEM}**	**$Log_{10}Dh_{ROOT}$**	**$Log_{10}(t/b)^2$**	**$Log_{10}CWT_{LW}$**	**$Log_{10}HCUE$**
Intercept (A)	**0.82 ± 0.06*****	**1.45 ± 0.05*****	**−1.52 ± 0.04*****	**0.49 ± 0.02*****	**−18.34 ± 0.07*****
$Log_{10}L$ (A)	**0.18 ± 0.01*****	**0.04 ± 0.02***	**−0.13 ± 0.01*****	**0.04 ± 0.01*****	**0.3 ± 0.02*****
$Log_{10}Dh_{APEX}$ (A)	**0.15 ± 0.06****	–	–	–	–
A_{2001}	–	**0.03 ± 0.01****	0.03 ± 0.03	−0.04 ± 0.02	**−0.09 ± 0.05***
EC	–	0.00 ± 0.01	0.05 ± 0.04	−0.04 ± 0.03	0.08 ± 0.06
ECSW	–	**−0.06 ± 0.02*****	**−0.28 ± 0.06*****	**−0.15 ± 0.05****	**0.52 ± 0.11****
SW	–	**−0.04 ± 0.01*****	−0.05 ± 0.04	0.02 ± 0.03	−0.11 ± 0.07
PECSW	–	**−0.03 ± 0.02***	**−0.38 ± 0.09*****	**−0.25 ± 0.07*****	**0.75 ± 0.17*****
PEC	–	**−0.04 ± 0.02***	0.07 ± 0.12	−0.16 ± 0.09	**0.06 ± 0.2**
$Log_{10}L \times A_{2001}$	–	–	−0.01 ± 0.02	0.02 ± 0.01	**0.06 ± 0.03***
$Log_{10}L \times EC$	–	–	−0.03 ± 0.02	0.02 ± 0.01	−0.02 ± 0.03
$Log_{10}L \times ECSW$	–	–	**0.13 ± 0.03***	**0.08 ± 0.02*****	**−0.23 ± 0.05*****
$Log_{10}L \times SW$	–	–	0.01 ± 0.02	0.01 ± 0.02	0.04 ± 0.03
$Log_{10}L \times PECSW$	–	–	**0.15 ± 0.04*****	**0.10 ± 0.03*****	**−0.26 ± 0.08****
$Log_{10}L \times PEC$	–	–	−0.06 ± 0.05	0.05 ± 0.04	0.08 ± 0.09

*$p < .05$, **$p < .01$ and ***$p < .001$.

effects (Table 4, Figure 1e). Along the roots, *D*h was in general wider before 2001, whereas all treatment combinations except EC (elevated CO_2) showed a significant overall reduction in Dh_{ROOT} (Table 4, Figure 1f). Treatment effects on $(t/b)^2$ were found for the combination of soil warming and elevated CO_2 (ECSW), also after CO_2 fumigation ceased in 2009 (PECSW), as shown by a steeper increase in $(t/b)^2$ with increasing distance from the apex. The model results for CWT_{LW} were analogous to those for $(t/b)^2$ (Table 4, Figure 1g). Similarly, the axial scaling of HCUE was influenced by the same treatment combinations as $(t/b)^2$ and CWT_{LW}, but with inversed relationships. In addition, HCUE for A_{2001} was smaller at the stem apex (i.e. smaller intercept (a) but increased along the stem at a faster rate (larger (b) than for the same trees after they had grown taller, irrespective of treatments. PERPAR showed no significant axial variation, and the one-way ANOVA performed instead to test for treatment effects revealed that soil warming (SW) had a significant negative effect on the production of ray parenchyma ($p < .05$) but no other treatment effects were significant.

3.3 | Trait trade-offs during ontogeny and under treatments

Pairwise comparisons between functional traits using a power function revealed a significant trade-off between proxies of hydraulic efficiency and safety (*D*h vs. $(t/b)^2$) (Figure 3), which seems partly due to their link through tracheid diameter. The slope *b* of the relationship $Log_{10}Dh = Log_{10}\ a + b \cdot Log_{10}\ (t/b)^2$ became less negative with increasing cambial age in stems and roots, respectively; Figure 3), independent from treatment with the exception of PECSW in the stem, which showed no ontogenetic trend ($p > .05$). Furthermore, stem hydraulic efficiency (*D*h) was negatively linked (*b*-values predominantly <0) to mechanical support (CWT_{LW}) with no significant change related to cambial age or treatment (Figure 3). In contrast, $(t/b)^2$ and CWT_{LW} were unrelated in the stem (slope *b* scattered around 0) and positively related in the roots (*b*-values mostly >0) with no ontogenetic trend or treatment effect (Figure 3). The pairwise relationship of PERPAR with the other functional traits was only assessed globally because of the reduced dataset (only data for 2000, 2006 and 2011) and revealed no significant relationship (Figure S5).

3.4 | Hydraulic efficiency: costs and effect on growth

The analyses of HCUE, the ratio between hydraulic conductance and structural carbon costs, indicated that, per unit of conductance, construction costs increase with height along the stem (Figure 4, Table 3).

Of all the considered functional traits, only the hydraulic diameter at the stem apex (Dh_{APEX}) had a significant effect ($p < .001$) on growth (Figure 5; other data not shown). Indeed, Dh_{APEX} explained 31% and 36% of the total variance in ΔH and RAI, respectively, independent from ontogeny and treatment ($p > .05$).

4 | DISCUSSION

4.1 | Axial scaling of functional traits is linked to biophysical principles

Our description of xylem anatomical traits showed characteristic axial scaling that can be attributed to different biophysical principles. As

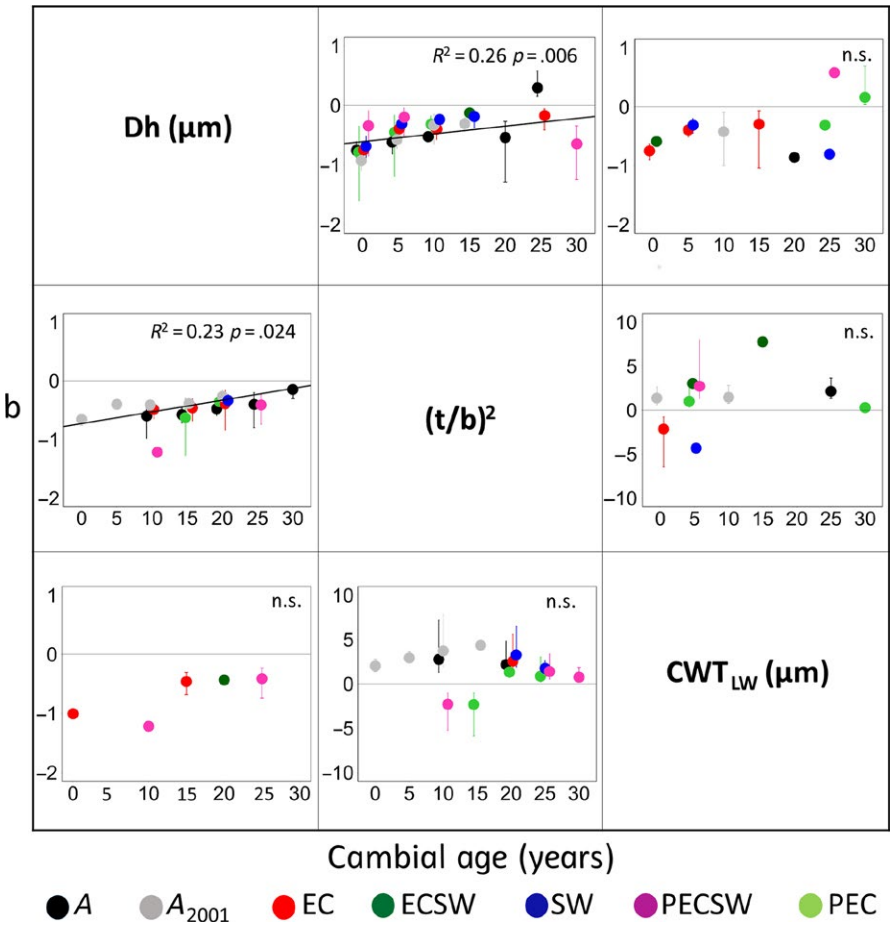

FIGURE 3 Power scaling exponent *b* of the pairwise relationships between *D*h, $(t/b)^2$ and CWT_{LW} as a function of cambial age of the tree rings in the stem (upper plots) and root (lower plots). Each symbol represents *b* ± 95% CI for all rings per 5-year cambial age class and treatment as obtained from RMA power fitting models. Power functions were used because they showed the best fit among the tested functions. A negative value of *b* indicates a trade-off, a positive value a collinear change between any two considered functional traits. Solid lines indicate the significant ($p < .05$) linear regression through all points irrespective of treatment as there were no treatment differences in the slope except for PECSW (post-CO_2 soil warming) in the stem *D*h vs. $(t/b)^2$ relationship

expected, the hydraulic efficiency (*D*h) scaled along the stem following a power function with a scaling exponent ($b = 0.17$) very similar to values reported in other studies (Anfodillo et al., 2013; Petit et al., 2011). This supports the remarkable universality of the axial conduit widening in vascular plants (Anfodillo, Carraro, Carrer, Fior, & Rossi, 2006; Olson et al., 2014; West et al., 1999) here demonstrated for the first time for trees subject to experimental manipulation of environmental conditions. Furthermore, in all trees and under all treatment combinations, xylem tracheids in the roots were wider than along the stem, in agreement with previous studies (McElrone, Pockman, Martinez-Vilalta, & Jackson, 2004; Petit, Anfodillo, & De Zan, 2009; Petit, Pfautsch, Anfodillo, & Adams, 2010). This strict axial configuration represents a biophysical optimization to buffer the increasing hydraulic resistance due to a longer path length as trees grow taller (Petit & Anfodillo, 2009; West et al., 1999). Instead, the cell wall reinforcement $(t/b)^2$ of the earlywood increased towards the apex, i.e. in parallel with the decrease in the water potential towards the apex (Domec, Pruyn, & Gartner, 2005). This is in line with previous findings showing a decrease with tree age and increase with height (Domec et al., 2009). The latewood cell wall thickness (CWT_{LW}) increased from stem apex to base (Figure 1c), thus indicating an increasing need for mechanical support by the latewood along the stem. Such mechanically stronger latewood cells might be required to compensate for the decreasing contribution of the earlywood to ring-level mechanical support towards the stem base as earlywood tracheid diameter increases. However, this increase was relatively small compared to, for example, the increase in accumulated biomass to the power of three to four when moving down the stem, as reconstructed for an individual of *Abies procera* (King, 2011), thus suggesting a nonlinear relationship between cell wall thickness and the mechanical support provided.

In contrast to the other functional tracheid traits, we did not find a consistent or clearly defined axial trend for the percent area of ray parenchyma (PERPAR) as expected. Indeed, an increase in ray size with age and distance from the stem apex, following the increase in tracheid size, would be expected (Lev-Yadun & Aloni, 1995). The variability along the stem axis was very large both between and within trees (ranging from 0.12% to 2.55%). This finding confirms previous observations that the ray proportion of conifers varies widely, both among individuals (Fonti et al., 2015; von Arx et al., 2017) and within the stem (Baker et al., 2000; DeSmidt, 1922; von Arx et al., 2015), with only a relatively weak influence of environmental conditions (Esteban, Martín, de Palacios, & Fernández, 2012; Olano et al., 2013) and/or functional needs such as storage space requirements (von Arx et al., 2017).

Generally, the trends observed in the roots were consistent with those observed in the stem but were much weaker, probably because roots are buffered against much of the above-ground environmental variability and also more responsive to soil geomorphic processes (Gärtner, Schweingruber, & Dikau, 2001). This increased

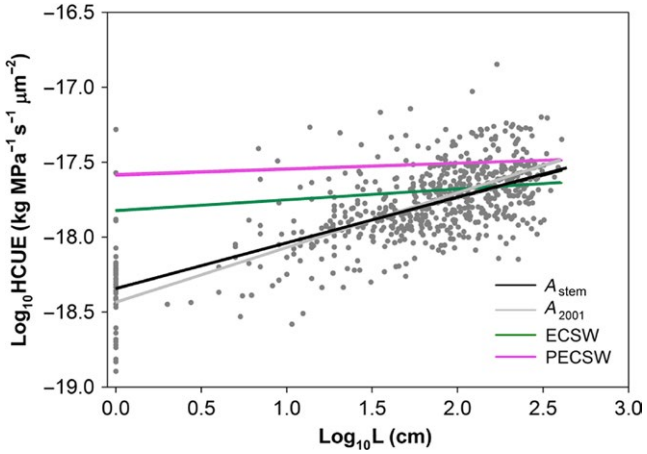

FIGURE 4 Variability of hydraulic carbon use efficiency (HCUE) with increasing distance from the apex (*L*), based on $\log_{10}$-transformed data. The black line refers to the HCUE trend of control trees only, whereas coloured lines indicate the significant treatment effects (see Table 3 for details)

variability might be because, compared to stems, roots have additional functions (e.g.flexibility, stiffness, anchorage) within a less homogeneous medium (different soil texture and depth) (Gärtner et al., 2001).

4.2 | Hydraulic efficiency shows no ontogenetic trend but a trade-off with hydraulic safety

During ontogeny, adjustments of the xylem structure are necessary to meet the changing functional needs as tree size increases. Despite these expected modifications, the power fitting observed for hydraulic efficiency (*D*h) appeared to be stable and independent from the ontogenetic tree development, suggesting strong biophysical control over the axial design of hydraulic efficiency. In contrast, hydraulic safety ($(t/b)^2$) showed a slight change in the axial scaling, which suggests a decrease in safety with increasing tree size. A possible explanation for this ontogenetic trend is that larger trees have a deeper root system with better access to soil water (Rosner, 2013). Similarly, at least when using power fitting, the axial scaling of the mechanical support (CWT_{LW}) changed in a way that suggested an increase during the course of a tree's life for a given distance from the apex. This may reflect size-related changes in tree architecture, since many trees invest increasingly into lateral structures as they grow taller, which requires stronger wood to support it (King, 2011).

Limited resources to form wood and differing biophysical constraints inherently imply trade-offs between the xylem functional needs, as demonstrated by the competing axial structural adjustments observed in our study (Figure 2). Specifically, and as hypothesized, we confirmed the presence of a trade-off between hydraulic efficiency and safety (Bouche et al., 2014; Gleason et al., 2016; Hacke, 2015; Sperry, Meinzer, & McCulloh, 2008). In addition, hydraulic efficiency was negatively related to mechanical stability. The observed hydraulic efficiency vs. safety trade-off is related to the fact that tracheids with narrow lumina are less efficient in transporting water but more resistant to implosion and xylem cavitation (Gleason et al., 2016). Our results suggest that this relationship changes along the stem axis in order to prioritize safety towards the stem apex and efficiency towards the stem base (Figure 2). This result is supported by the fact that the construction costs for the hydraulic system (HCUE, i.e. the hydraulic conductance per unit of cell wall area) were higher towards the stem apex (Figure 4, Table 3). This could be explained by the importance of an undamaged apex to sustain height growth and compete with neighbouring trees, particularly in a conifer with clear apical dominance such as *L. decidua*.

4.3 | Environmental conditions have a differential impact on functional traits

Previous studies suggested that *L. decidua* responded more to elevated CO_2 than soil warming (Dawes et al., 2011, 2015; Handa

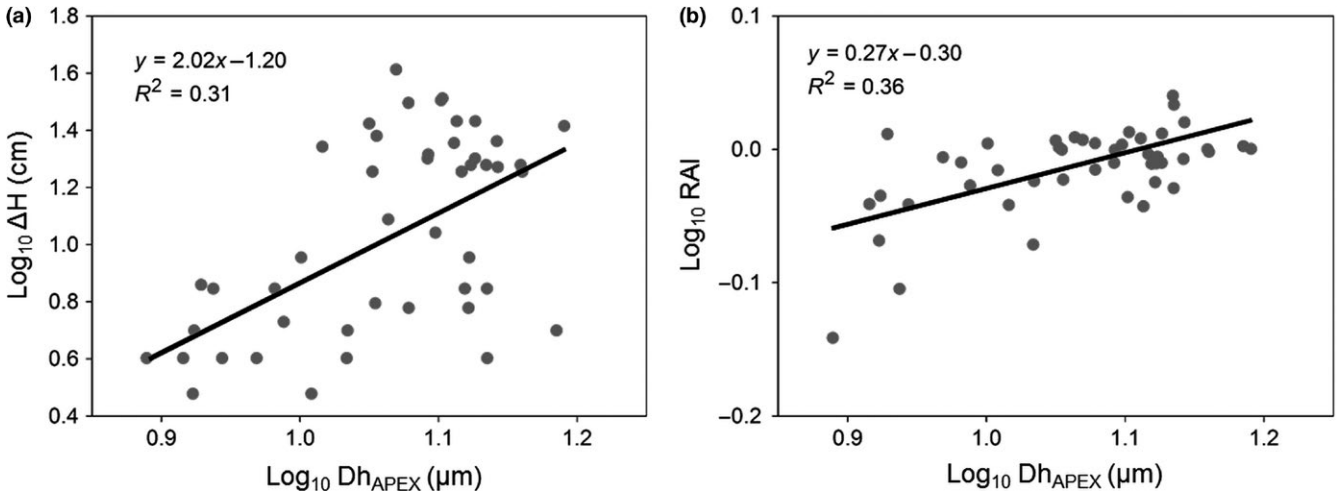

FIGURE 5 Relationship between the mean hydraulic diameter of apical tracheids (Dh_{APEX}: *D*h at $L \leq 1$ cm) and (a) ΔH (annual stem elongation rate) and (b) RAI (ring area index, i.e. the ring area (RA) at the stem base standardized to remove the general axial pattern of RA vs. *L*, see Table 2). Solid lines represent the fitted linear regressions

et al., 2006), e.g. by increased above-ground growth (Dawes et al., 2011, 2015), including greater leaf canopy (Streit et al., 2014) and increased accumulation of non-structural carbohydrates (Handa, Körner, & Hättenschwiler, 2005; Hättenschwiler et al., 2002). Our results suggest that soil warming and elevated CO_2 did not strongly influence the scaling of the analysed functional traits along the stem (Table 3). As hypothesized, effects of environmental conditions emerged only in the functional traits that did not show a very strong biophysical determination, for example the mean hydraulic diameter in the roots (Dh_{ROOT}) and the percent area of ray parenchyma (PERPAR). Specifically, the soil warming treatment had a local effect restricted to root xylem anatomy. The significant decrease in Dh_{ROOT} under soil warming implies reduced overall root conductance because no significant compensating increase in root biomass was observed (Dawes et al., 2015). However, when considering that a 4°C increase in water temperature lowers viscosity and thus hydraulic resistance by *c*. 12% according to the Hagen-Poiseuille equation (Tyree & Zimmermann, 2002), the observed increase in hydraulic resistance due to slightly smaller Dh_{ROOT} is in roughly the same range, thus resulting in a net effect close to zero. In any case, due to the comparably minimal hydraulic resistance of the wide root tracheids, such a small decrease in lumen size has almost no effect on overall pathway length resistance and therefore likely no functional relevance for whole plant conductance, transpiration and photosynthesis. Soil warming also reduced $PERPAR_{STEM}$ but not $PERPAR_{ROOT}$. However, tree line trees are usually relatively rich in NSCs and starch reserves (Hoch & Körner, 2012), and the different warming effects on PERPAR in the stem and roots may reflect an osmotic adjustment of the root-to-leaf gradient of water potential that effectively influences the translocation of sugars within the plant (Dawes, Zweifel, Dawes, Rixen, & Hagedorn, 2014; Hölttä, Vesala, Sevanto, Perämäki, & Nikinmaa, 2006).

Furthermore, our results showed a weak increase in $(t/b)^2$ and CWT_{LW} with increasing distance from apex (*L*) under ECSW and PECSW, meaning that trees profited from the larger amount of photosynthates available under elevated CO_2, by having a greater needle biomass (Dawes et al., 2015) and by increasing the mechanical stability of the trunk (Figure 1f,g). At the same time, the significantly lower values of $(t/b)^2$ and CWT_{LW} close to the stem apex under CO_2 enrichment could explain the increase in freezing sensitivity of trees exposed to elevated CO_2, particularly in taller trees, as previously observed for the period 2005–2010 (Martin, Gavazov, Körner, Hättenschwiler, & Rixen, 2010; Rixen, Dawes, Wipf, & Hagedorn, 2012).

4.4 | Greater mean hydraulic diameter at the apex promotes growth

The observed within-tree variability of anatomical traits and its influence on tree functioning lead to the obvious question about the relevance for growth. Of all the functional traits analysed in this respect, only the mean hydraulic diameter at the stem apex (Dh_{APEX}) was important, explaining 31% and 36% of the variability in stem elongation and ring area at the stem base, respectively (Figure 5). This result highlights the importance of hydraulic efficiency for growth. More specifically, the finding that Dh_{APEX}, and not Dh_{STEM} or Dh_{ROOT}, was significant is remarkable. Indeed, the apex is a hydraulic bottleneck restricting growth (Petit & Anfodillo, 2009; Petit et al., 2011; West et al., 1999), and previous studies showed that Dh_{APEX} increases slightly as trees grow taller, presumably to counteract the concomitant increase in water tension accompanying height growth (Olson et al., 2014; Petit, Anfodillo, & Mencuccini, 2008). Our results are thus in line with these studies and support the view that an increase in the conductivity of the stem apex releases the hydraulic constraints on water transport, thus favouring gas exchange and ultimately growth (Petit et al., 2011).

5 | CONCLUSIONS

In this study, we quantified xylem anatomical traits in tree rings along the stem and root axis and derived corresponding xylem functions to identify priorities and trade-offs and to determine if ontogeny or experimental manipulation of CO_2 and temperature influence these relationships. The strong biophysical constraints resulted in a narrowly confined axial pattern of *D*h, suggesting a prioritization of hydraulic efficiency over other xylem functions (hydraulic safety, mechanical support, metabolic functions). Likewise, at the apex, a tree's hydraulic bottleneck, a small increase in *D*h significantly enhances water transport, thus fuelling carbon assimilation supporting growth. The higher variability of the other functional traits potentially indicates a greater ability or need to respond to the environment and ontogenetic development. Moreover, our findings indicate that the overall architectural design of the tree requires a certain priority of hydraulic safety towards the stem apex, while hydraulic efficiency and mechanical support gain progressively more importance towards the stem base. In conclusion, our study suggests that prioritized xylem functional traits show a very strong biophysical determination, while subordinate traits respond more plastically to intrinsic and extrinsic factors.

ACKNOWLEDGEMENTS

We thank S. Hättenschwiler for initiating and F. Hagedorn for running the 12-year CO_2 enrichment and soil warming experiment, as well as many colleagues at the WSL and SLF for assistance with field work and technical support. We acknowledge S. Lechthaler in particular for helping with measurements on tangential sections. Major funding sources for this tree line experiment included the Swiss National Science Foundation from 2001–2005 (grant 31-061428.00 to S. Hättenschwiler) and Swiss National Science Foundation from 2007–2010 (grant 315200-116861 to CR); the Velux Foundation from 2007 to 2012 (grant 371 to F. Hagedorn); and the WSL from 2012 to 2016 (grant to CR and MAD). This particular study was supported by the COST Action F1106 "Studying Tree Responses to extreme Events". GvA was supported by grants from the Swiss State Secretariat for Education, Research and Innovation SERI (SBFI C14.0104 and C12.0100).

AUTHORS' CONTRIBUTIONS

All authors planned and designed the research, and C.R., M.A.D., and P.F. conducted the fieldwork; A.L.P. collected the data; A.L.P., G.P., P.F., and G.v.A. analysed the data; A.L.P. led the manuscript drafting with contributions from G.P., P.F., and G.v.A. All authors discussed, revised and approved the manuscript.

DATA ACCESSIBILITY

Data are deposited in the Dryad Digital Repository https://doi.org/10.5061/dryad.k6516 (Prendin, Petit, & Fonti et al., 2017).

ORCID

Angela Luisa Prendin http://orcid.org/0000-0002-5809-7314
Giai Petit http://orcid.org/0000-0002-6546-7141
Patrick Fonti http://orcid.org/0000-0002-7070-3292
Christian Rixen http://orcid.org/0000-0002-2486-9988
Melissa Autumn Dawes http://orcid.org/0000-0003-4919-0151
Georg von Arx http://orcid.org/0000-0002-8566-4599

REFERENCES

Anderegg, W. R. L., Plavcová, L., Anderegg, L. D. L., Hacke, U. G., Berry, J. A., & Field, C. B. (2013). Drought's legacy: Multiyear hydraulic deterioration underlies widespread aspen forest die-off and portends increased future risk. *Global Change Biology*, *19*, 1188–1196.

Anfodillo, T., Carraro, V., Carrer, M., Fior, C., & Rossi, S. (2006). Convergent tapering of xylem conduits in different woody species. *New Phytologist*, *169*, 279–290.

Anfodillo, T., Petit, G., & Crivellaro, A. (2013). Axial conduit widening in woody species: A still neglected anatomical pattern. *IAWA Journal*, *34*, 352–364.

Baker, D. C., Spicer, R., & Gartner, B. L. (2000). Distribution and vitality of xylem rays in relation to tree leaf area in Douglas-fir. *IAWA Journal*, *21*, 389–401.

Bannan, M. W. (1937). Observations on the distribution of xylem-ray tissue in conifers. *Annals of Botany*, *1*, 717–726.

Barbeito, I., Dawes, M. A., Rixen, C., Senn, J., & Bebi, P. (2012). Factors driving mortality and growth at treeline: A 30-year experiment of 92000 conifers. *Ecology*, *93*, 389–401.

Barton, K., & Barton, M. K. (2013). MuMIn: multi-model interference. R Package version 1.9.5. Retrived from http://r-forge.r-project.org/projects/mumin/10/6/2013

Bates, D., Mächler, M., Bolker, B., & Walker, S. (2015). Fitting linear mixed-effects models using lme4. *Journal of Statistical Software*, *67*, 1–48.

Beeckman, H. (2016). Wood anatomy and trait-based ecology. *IAWA Journal*, *37*, 127–151.

Bittencourt, P. R. L., Pereira, L., & Oliveira, R. S. (2016). On xylem hydraulic efficiencies, wood space-use and the safety-efficiency tradeoff. *New Phytologist*, *211*, 1152–1155.

Björklund, J., Seftigen, K., Schweingruber, F., Fonti, P., von Arx, G., Bryukhanova, M. V., … Frank, D. C. (2017). Cell size and wall dimensions drive distinct variability of earlywood and latewood density in Northern Hemisphere conifers. *New Phytologist*, https://doi.org/10.1111/nph.14639

Bouche, P. S., Larter, M., Domec, J. C., Burlett, R., Gasson, P., Jansen, S., & Delzon, S. (2014). A broad survey of hydraulic and mechanical safety in the xylem of conifers. *Journal of Experimental Botany*, *65*, 4419–4431.

Brodersen, C. R., & McElrone, A. J. (2013). Maintenance of xylem network transport capacity: A review of embolism repair in vascular plants. *Frontiers in Plant Science*, *4*, 1–11.

Burnham, K. P., & Anderson, D. R. (2002). Ecological modelling. *Model selection and multimodel inference a practical information-theoretic approach*, (2nd ed.) New York, NY: Springer-Verlag Inc.

Choat, B. (2013). Predicting thresholds of drought-induced mortality in woody plant species. *Tree Physiology*, *33*, 669–671.

Dawes, M. A., Hättenschwiler, S., Bebi, P., Hagedorn, F., Handa, I. T., Körner, C., & Rixen, C. (2011). Species-specific tree growth responses to 9 years of CO_2 enrichment at the alpine treeline. *Journal of Ecology*, *99*, 382–394.

Dawes, M. A., Philipson, C. D., Fonti, P., Bebi, P., Hättenschwiler, S., Hagedorn, F., & Rixen, C. (2015). Soil warming and CO_2 enrichment induce biomass shifts in alpine tree line vegetation. *Global Change Biology*, *21*, 2005–2021.

Dawes, M. A., Zweifel, R., Dawes, N., Rixen, C., & Hagedorn, F. (2014). CO_2 enrichment alters diurnal stem radius fluctuations of 36-year-old *Larix decidua* growing at the alpine tree line. *New Phytologist*, *202*, 1237–1248.

Denne, M. P. (1988). Definition of latewood according to Mork (1928). *IAWA Journal*, *10*, 59–62.

DeSmidt, W. J. (1922). Studies of the distribution and volume of the wood rays in slippery elm (*Ulmus Fulva* Michx.). *Journal of Forestry*, *20*, 352–362.

Domec, J.-C., & Gartner, B. L. (2002). How do water transport and water storage differ in coniferous earlywood and latewood? *Journal of Experimental Botany*, *53*, 2369–2379.

Domec, J.-C., Lachenbruch, B., Meinzer, F. C., Woodruff, D. R., Warren, J. M., & McCulloh, K. A. (2008). Maximum height in a conifer is associated with conflicting requirements for xylem design. *Proceedings of the National Academy of Sciences of the United States of America*, *105*, 12069–12074.

Domec, J. C., Pruyn, M. L., & Gartner, B. L. (2005). Axial and radial profiles in conductivities, water storage and native embolism in trunks of young and old-growth ponderosa pine trees. *Plant, Cell & Environment*, *28*, 1103–1113.

Domec, J.-C., Warren, J. M., Meinzer, F. C., & Lachenbruch, B. (2009). Safety factors for xylem failure by implosion and air-seeding within roots, trunks and branches of young and old conifer trees. *IAWA Journal*, *30*, 101–120.

Esteban, L. G., Martín, J. A., de Palacios, P., & Fernández, F. G. (2012). Influence of region of provenance and climate factors on wood anatomical traits of *Pinus nigra* Arn. subsp. *salzmannii*. *European Journal of Forest Research*, *131*, 633–645.

Fatichi, S., Leuzinger, S., & Körner, C. (2014). Moving beyond photosynthesis: From carbon source to sink-driven vegetation modeling. *New Phytologist*, *201*, 1086–1095.

Fatichi, S., Rimkus, S., Burlando, P., Bordoy, R., & Molnar, P. (2013). Elevational dependence of climate change impacts on water resources in an Alpine catchment. *Hydrology and Earth System Sciences Discussions*, *10*, 3743–3794.

Finto, A., Schimleck, L., & Daniels, R. (2012). A comparison of earlywood-latewood demarcation methods–A case study in loblolly pine. *IAWA Journal*, *33*, 187–195.

Fonti, P., & Jansen, S. (2012). Xylem plasticity in response to climate. *New Phytologist*, *195*, 734–736.

Fonti, P., Tabakova, M. A., Kirdyanov, A. V., Bryukhanova, M. V., & von Arx, G. (2015). Variability of ray anatomy of *Larix gmelinii* along a forest productivity gradient in Siberia. *Trees*, *29*, 1165–1175.

Fonti, P., von Arx, G., García-González, I., Eilmann, B., Sass-Klaassen, U., Gärtner, H., & Eckstein, D. (2010). Studying global change through investigation of the plastic responses of xylem anatomy in tree rings. *New Phytologist*, *185*, 42–53.

Gärtner, H., Schweingruber, F. H., & Dikau, R. (2001). Determination of erosion rates by analyzing structural changes in the growth pattern of exposed roots. *Dendrochronologia*, *19*, 81–91.

Gleason, S. M., Westoby, M., Jansen, S., Choat, B., Hacke, U. G., Pratt, R. B., … Zanne, A. E. (2016). Weak tradeoff between xylem safety and xylem-specific hydraulic efficiency across the world's woody plant species. *New Phytologist*, *209*, 123–136.

Hacke, U. (2015). *Functional and ecological xylem anatomy* (ed. U. Hacke). Cham, Switzerland: Springer International Publishing.

Hacke, U. G., Sperry, J. S., Pockman, W. T., Davis, S. D., & McCulloh, K. A. (2001). Trends in wood density and structure are linked to prevention of xylem implosion by negative pressure. *Oecologia*, *126*, 457–461.

Hagedorn, F., Martin, M. A., Rixen, C., Rusch, S., Bebi, P., Zürcher, A., … Hättenschwiler, S. (2010). Short-term responses of ecosystem carbon fluxes to experimental soil warming at the Swiss alpine treeline. *Biogeochemistry*, *97*, 7–19.

Handa, I. T., Körner, C., & Hättenschwiler, S. (2005). A test of the treeline carbon limitation hypotesis by in situ CO_2 enrichment and defoliation. *Functional Ecology*, *86*, 1288–1300.

Handa, I. T., Körner, C., & Hättenschwiler, S. (2006). Conifer stem growth at the altitudinal treeline in response to four years of CO_2 enrichment. *Global Change Biology*, *12*, 2417–2430.

Harsch, M. A., Hulme, P. E., McGlone, M. S., & Duncan, R. P. (2009). Are treelines advancing? A global meta-analysis of treeline response to climate warming. *Ecology Letters*, *12*, 1040–1049.

Hättenschwiler, S., Handa, I. T., Egli, L., Asshoff, R., Ammann, W., & Körner, C. (2002). Atmospheric CO_2 enrichment of alpine treeline conifers. *New Phytologist*, *156*, 363–375.

Hoch, G., & Körner, C. (2012). Global patterns of mobile carbon stores in trees at the high-elevation tree line. *Global Ecology and Biogeography*, *21*, 861–871.

Hölttä, T., Vesala, T., Sevanto, S., Perämäki, M., & Nikinmaa, E. (2006). Modeling xylem and phloem water flows in trees according to cohesion theory and Münch hypothesis. *Trees*, *20*, 67–78.

Jyske, T., Mäkinen, H., & Saranpää, P. (2008). Wood density within Norway Spruce stems. *Silva Fennica*, *42*, 439–455.

King, D. A. (2011). Size-related changes in tree proportions and their potential influence on the course of height growth. In F. C. Meinzer, B. Lachenbruch, & T. E. Dawson (Eds.), *Tree physiology* (pp. 165–191). Dordrecht, The Netherlands: Springer.

Koch, G. W., Sillett, S. C., Jennings, G. M., & Davis, S. D. (2004). The limits to tree height. *Nature*, *428*, 851–854.

Kolb, K. J., & Sperry, J. S. (1999). Transport constraints on water use by the Great Basin shrub, *Artemisia tridentata*. *Plant, Cell & Environment*, *22*, 925–935.

Körner, C. (2012). *Alpine treelines*. Basel, Switzerland: Springer Basel.

Koubaa, A., Zhang, S. Y. T., & Makni, S. (2002). Defining the transition from earlywood to latewood in black spruce based on intra-ring wood density profiles from X-ray densitometry. *Annals of Forest Science*, *59*, 511–518.

Lachenbruch, B., & McCulloh, K. A. (2014). Traits, properties, and performance: How woody plants combine hydraulic and mechanical functions in a cell, tissue, or whole plant. *New Phytologist*, *204*, 747–764.

Larson, P. R. (1963). Stem form development of forest trees. *Forest Science*, *9*, a0001.

Lazzarin, M., Crivellaro, A., Williams, C. B., Dawson, T. E., Mozzi, G., & Anfodillo, T. (2016). Tracheid and pit anatomy vary in tandem in a tall *Sequoiadendron giganteum* tree. *IAWA Journal*, *37*, 172–185.

Legendre, P. (2014). lmodel2: Model II regression. R package version 1.7-2. Retrived from http://CRAN.R-project.org/package=lmodel2

Lev-Yadun, S., & Aloni, R. (1995). Differentiation of the ray system in woody plants. *The Botanical Review*, *61*, 45–84.

Lintunen, A., Paljakka, T., Jyske, T., Peltoniemi, M., Sterck, F., von Arx, G., … Hölttä, T. (2016). Osmolality and non-structural carbohydrate composition in the secondary phloem of trees across a latitudinal gradient in Europe. *Frontiers in Plant Science*, *7*, 726.

Lundgren, C. (2004). Cell wall thickness and tangential and radial cell diameter of fertilized and irrigated Norway spruce. *Silva Fennica*, *38*, 95–106.

Martin, M., Gavazov, K., Körner, C., Hättenschwiler, S., & Rixen, C. (2010). Reduced early growing season freezing resistance in alpine treeline plants under elevated atmospheric CO_2. *Global Change Biology*, *16*, 1057–1070.

Mcculloh, K. A., Johnson, D. M., Meinzer, F. C., & Woodruff, D. R. (2014). The dynamic pipeline : Hydraulic capacitance and xylem hydraulic safety in four tall conifer species. *Plant, Cell & Environment*, *37*, 1171–1183.

McElrone, A. J., Pockman, W. T., Martinez-Vilalta, J., & Jackson, R. B. (2004). Variation in xylem structure and function in stems and roots of trees to 20 m depth. *New Phytologist*, *163*, 507–517.

Meinzer, F. C., Lachenbruch, B., & Dawson, T. E. (2011). *Size- and age-related changes in tree structure and function*. Dordrecht, The Netherlands: Springer.

Mencuccini, M., Grace, J., & Fioravanti, M. (1997). Biomechanical and hydraulic determinants of tree structure in Scots pine: Anatomical characteristics. *Tree Physiology*, *17*, 105–113.

Mitchell, M. D., & Denne, M. P. (1997). Variation in density of *Picea sitchensis* in relation to within-tree trends in tracheid diameter and wall thickness. *Forestry*, *70*, 47–60.

Myburg, A. A., Lev-Yadun, S., & Sederoff, R. R. (2013). *Xylem structure and function. eLS* (pp. 1–9). Chichester, UK: John Wiley & Sons, Ltd.

Nardini, A., Lo Gullo, M. A., & Salleo, S. (2011). Refilling embolized xylem conduits: Is it a matter of phloem unloading? *Plant Science*, *180*, 604–611.

Niklas, K. J. (2007). Maximum plant height and the biophysical factors that limit it. *Tree Physiology*, *27*, 433–440.

Niklas, K. J., & Spatz, H. (2004). Growth and hydraulic (not mechanical) constraints govern the scaling of tree height and mass. *Proceedings of the National Academy of Sciences of the United States of America*, *101*, 15661–15663.

Olano, J. M., Arzac, A., García-Cervigón, A. I., von Arx, G., & Rozas, V. (2013). New star on the stage: Amount of ray parenchyma in tree rings shows a link to climate. *New Phytologist*, *198*, 486–495.

Olson, M. E., Anfodillo, T., Rosell, J. A., Petit, G., Crivellaro, A., Isnard, S., … Castorena, M. (2014). Universal hydraulics of the flowering plants: Vessel diameter scales with stem length across angiosperm lineages, habits and climates. *Ecology Letters*, *17*, 988–997.

Petit, G., & Anfodillo, T. (2009). Plant physiology in theory and practice: An analysis of the WBE model for vascular plants. *Journal of Theoretical Biology*, *259*, 1–4.

Petit, G., Anfodillo, T., Carraro, V., & Grani, F. (2011). Hydraulic constraints limit height growth in trees at high altitude. *New Phytologist*, *241–252*, 241–252.

Petit, G., Anfodillo, T., & De Zan, C. (2009). Degree of tapering of xylem conduits in stems and roots of small *Pinus cembra* and *Larix decidua* trees. *Botany-Botanique*, *87*, 501–508.

Petit, G., Anfodillo, T., & Mencuccini, M. (2008). Tapering of xylem conduits and hydraulic limitations in sycamore (*Acer pseudoplatanus*) trees. *New Phytologist*, *177*, 653–664.

Petit, G., Pfautsch, S., Anfodillo, T., & Adams, M. A. (2010). The challenge of tree height in *Eucalyptus regnans*: When xylem tapering overcomes hydraulic resistance. *New Phytologist*, *187*, 1146–1153.

Pfautsch, S., Hölttä, T., & Mencuccini, M. (2015). Hydraulic functioning of tree stems – fusing ray anatomy, radial transfer and capacitance. *Tree Physiology*, *35*, 706–722.

Pinheiro, J. C., & Bates, D. M. (2000). Linear mixed-effects models: Basic concepts and examples. In J. Chambers, W. Eddy, W. Härdle, S. Sheather, & L. Tierney (Eds.), *Mixed effects models in S and S-plus* (pp. 1–271). New York, NY: Springer.

Pittermann, J., Sperry, J. S., Wheeler, J. K., Hacke, U. G., & Sikkema, E. H. (2006). Mechanical reinforcement of tracheids compromises the hydraulic efficiency of conifer xylem. *Plant, Cell and Environment*, *29*, 1618–1628.

Prendin, A. L., Petit, G., Carrer, M., Fonti, P., Björklund, J., & von Arx, G. (2017). New research perspectives from a novel approach to quantify tracheid wall thickness. *Tree Physiology*, *37*, 976–983.

Prendin, A. L., Petit, G., Fonti, P., Rixen, C., Dawes, M. A., & von Arx, G. (2017). Data from: Axial xylem architecture of *Larix decidua* exposed to CO_2 enrichment and soil warming at the tree line. *Dryad Digital Repository*, https://doi.org/10.5061/dryad.k6516

R Development Core Team. (2014). R: A language and environment for statistical computing. Vienna, Austria: R Foundation for Statistical Computing. Retrieved from http://www.R-project.org/.

Rixen, C., Dawes, M. A., Wipf, S., & Hagedorn, F. (2012). Evidence of enhanced freezing damage in treeline plants during six years of CO_2 enrichment and soil warming. *Oikos*, *121*, 1532–1543.

Rosner, S. (2013). Hydraulic and biomechanical optimization in norway spruce trunkwood – A review. *IAWA Journal*, *34*, 365–390.

Rosner, S., & Karlsson, B. (2011). Hydraulic efficiency compromises compression strength perpendicular to the grain in Norway spruce trunkwood. *Trees – Structure and Function*, *25*, 289–299.

Salleo, S., Trifilò, P., Esposito, S., Nardini, A., & Lo Gullo, M. A. (2009). Starch-to-sugar conversion in wood parenchyma of field-growing *Laurus nobilis* plants: A component of the signal pathway for embolism repair? *Functional Plant Biology*, *36*, 815.

Savage, V. M., Bentley, L. P., Enquist, B. J., Sperry, J. S., Smith, D. D., Reich, P. B., & von Allmen, E. I. (2010). Hydraulic trade-offs and space filling enable better predictions of vascular structure and function in plants. *Proceedings of the National Academy of Sciences of the United States of America*, *107*, 22722–22727.

Schönenberger, W., & Frey, W. (1988). Untersuchungen zur Okologie und Technik der Hochlagenaufforstung. For- schungsergebnisse aus dem Lawinenanrissgebiet Stillberg. *Swiss Forestry Journal*, *139*, 735–820.

Sperry, J. S., Meinzer, F. C., & McCulloh, K. A. (2008). Safety and efficiency conflicts in hydraulic architecture: Scaling from tissues to trees. *Plant, Cell & Environment*, *31*, 632–645.

Sperry, J. S., Nichols, K. L., Sullivan, J. E. M., & Eastlack, S. E. (1994). Xylem embolism in ring-porous, diffuse-porous, and coniferous trees of Northern Utah and interior Alaska. *Ecology*, *75*, 1736–1752.

Spicer, R. (2014). Symplasmic networks in secondary vascular tissues: Parenchyma distribution and activity supporting long-distance transport. *Journal of Experimental Botany*, *65*, 1829–1848.

Streit, K., Siegwolf, R. T. W., Hagedorn, F., Schaub, M., & Buchmann, N. (2014). Lack of photosynthetic or stomatal regulation after 9 years of elevated [CO_2] and 4 years of soil warming in two conifer species at the alpine treeline. *Plant, Cell & Environment*, *37*, 315–326.

Tyree, M. T., & Ewers, F. W. (1991). The hydraulic architecture of trees and other woody plants. *New Phytologist*, *119*, 345–360.

Tyree, M. T., & Zimmermann, M. H. (2002). *Xylem structure and the ascent of sap*. Berlin, Germany: Springer.

von Arx, G., Arzac, A., Fonti, P., Frank, D., Zweifel, R., Rigling, A., … Olano, M. (2017). Responses of sapwood ray parenchyma and non-structural carbohydrates of *Pinus sylvestris* to drought and long-term irrigation. *Functional Ecology*, *31*, 1371–1382.

von Arx, G., Arzac, A., Olano, J. M., & Fonti, P. (2015). Assessing conifer ray parenchyma for ecological studies: Pitfalls and guidelines. *Frontiers in Plant Science*, *6*, 1016.

von Arx, G., & Carrer, M. (2014). ROXAS – A new tool to build centuries-long tracheid-lumen chronologies in conifers. *Dendrochronologia*, *32*, 290–293.

von Arx, G., Crivellaro, A., Prendin, A. L., Čufar, K., & Carrer, M. (2016). Quantitative wood anatomy—Practical guidelines. *Frontiers in Plant Science*, *7*, 781.

von Arx, G., & Dietz, H. (2005). Automated image analysis of annual rings in the roots of perennial forbs. *International Journal of Plant Sciences*, *166*, 723–732.

West, G. B., Brown, J. H., & Enquist, B. J. (1999). A general model for the structure and allometry of plant vascular systems. *Nature*, *400*, 664–667.

Wimmer, R. (2002). Wood anatomical features in tree rings as indicators of environmental change. *Dendrochronologia*, *20*, 21–36.

Zar, J. H. (1999). *Biostatistical analysis* (4th edn). Upper Saddle River, NJ: Prentice-Hall.

Ziemińska, K., Westoby, M., & Wright, I. J. (2015). Broad anatomical variation within a narrow wood density range – A study of twig wood across 69 Australian angiosperms. *PLoS ONE*, *10*, e0124892.

Zuur, A. F., Ieno, E. N., Walker, N., Saveliev, A. A., & Smith, G. M. (2009). *Mixed effects models and extensions in ecology with R*. New York, NY: Springer.

SUPPORTING INFORMATION

Additional Supporting Information may be found online in the supporting information tab for this article.

How to cite this article: Prendin AL, Petit G, Fonti P, Rixen C, Dawes MA, von Arx G. Axial xylem architecture of *Larix decidua* exposed to CO_2 enrichment and soil warming at the tree line. *Funct Ecol*. 2018;32:273–287. https://doi.org/10.1111/1365-2435.12986